The Farthest Point Strategy for Progressive Image Sampling

Yuval Eldar, Michael Lindenbaum, *Member, IEEE,* Moshe Porat, *Senior Member, IEEE,* and Yehoshua Y. Zeevi

***Abstract*— A new method of farthest point strategy (FPS) for progressive image acquisition—an acquisition process that enables an approximation of the whole image at each sampling stage—is presented. Its main advantage is in retaining its uniformity with the increased density, providing efficient means for sparse image sampling and display. In contrast to previously presented stochastic approaches, the FPS guarantees the uniformity in a deterministic min-max sense. Within this uniformity criterion, the sampling points are irregularly spaced, exhibiting anti-aliasing properties comparable to those characteristic of the best available method (Poisson disk). A straightforward modification of the FPS yields an image-dependent adaptive sampling scheme. An efficient $O(N \log N)$ algorithm for both versions is introduced, and several applications of the FPS are discussed.**

***Index Terms*—Anti-aliasing, progressive sampling, progressive transmission.**

I. Introduction

THE task of progressive sampling of two-dimensional (2-D) data is considered. This task is of interest, for example, when the time required to sample or transmit all the data is too long, but a uniform approximation of the data may also be useful. In progressive sampling, the available 2-D data and the corresponding quality of this approximation increase with time. To enable such an approximation, we propose a method for generating a sequence of planar points with spatial distribution that is uniform for any number of samples. While the specific example of monochromatic image sampling is discussed, the results apply to many 2-D data acquisition applications such as terrain altitude measurements, range sensors, etc. The proposed algorithm is suitable for any 2-D data where the correlation between sample values decreases with the distance between the sample points, as is the case for most natural images.

The common raster scan fails to meet the fundamental requirement of progressive sampling—to provide an approximation of the whole image after each stage of the sampling process. In the raster scan and similar techniques, the scanned area data is revealed at the highest resolution, while the rest of the image remains completely unknown. The natural augmentation of the raster scan for progressive sampling purposes would be to sample the image on a series of rectangular grids with increasing resolution. The sample distribution obtained in the latter case after each stage is uniform, but the regularity of the grid usually yields annoying aliasing effects, especially at the first stages.

Aliasing is inherent in regular subsampling, unless the image is lowpass filtered to the appropriate bandwidth before it is sampled. For many applications such prefiltering is not feasible, and therefore irregular sampling is sometimes adopted. Note that a sampling pattern may be irregular and yet be uniform. Uniformity merely means that the sample density is approximately constant, thus providing an equal amount of information about every part of the image. Several works suggest to use stochastic sample distributions in order to break the pattern's regularity and avoid aliasing [6], [8], [15]. A more detailed description of this approach can be found in Section V. Unfortunately, the stochastic distribution that exhibits the best anti-aliasing properties—the Poisson disk distribution—cannot be easily fitted into a progressive sampling framework, since there is no obvious way to add points to the low resolution sample pattern and still retain the same spatial distribution. In this context we should mention the uniformly distributed deterministically generated indices (UDDI) scan, suggested in [9], [11], which is a pseudorandom space filling scan along congruent lines, resulting in a fairly uniform sample distribution after each stage.

We propose here a progressive sampling algorithm, called *farthest point sampling* (FPS), designed to provide a truly dynamic resolution. The main idea is to add one sample point at a time, and to place it in the middle of the least-known image area. The nonadaptive version of the algorithm generates an infinite sequence of uniformly distributed sample points. All the sample sets extracted from this sequence, at any size, comply with the same deterministic uniformity criterion. The uniformity of this irregular pattern leads to both high data acquisition rate and excellent anti-aliasing properties. An efficient algorithm for FPS implementation is also suggested, making it feasible and attractive for various applications.

Uniform distribution of the sample points seems to be the best *a priori* strategy, yet it is always suboptimal, since image data statistics are not stationary. A more sophisticated approach is to extract from the current sample set some

Manuscript received May 17, 1995; revised October 10, 1996. This work was supported in part by the Fund for the Promotion of Research at the Technion (050-890), by the Integrated Vision Platform Fund (050-899), and by the Ollendorff Research Fund. The associate editor coordinating the review of this manuscript and approving it for publication was Prof. Charles A. Bouman.

Y. Eldar is with IBM Israel Science and Technology, Haifa 31905, Israel.

M. Lindenbaum is with the Department of Computer Science, Technion–Israel Institute of Technology, Haifa 32000, Israel (e-mail: mic@cs.technion.ac.il).

M. Porat and Y. Y. Zeevi are with the Department of Electrical Engineering, Technion–Israel Institute of Technology, Haifa 32000, Israel (e-mail: mp@ee.technion.ac.il).

Publisher Item Identifier S 1057-7149(97)06250-7.

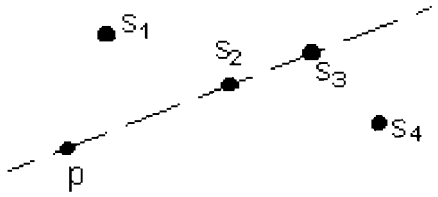

Fig. 1. Occluded point situation: $I_L(p)$ depends on the image values at s_1, s_2, and s_4, but not on $I(s_3)$, since s_3 is occluded by s_2. In the 1-D case, all sample points are colinear, hence the image interpolation over each unsampled segment is determined by the sample values at the segment's ends.

information about the image structure and adapt the sample density at each region to the local information content. Adaptive sampling can be introduced within the framework of the FPS by a minor change of the algorithm, yielding enhanced reconstruction with no additional computational cost.

II. The Farthest Point Strategy

All the progressive sampling methods mentioned above (except UDDI) take the same coarse-to-fine approach—some kind of uniform sampling is applied again and again in different resolutions. This paper suggests a different concept—adding one sample point at a time, with the key question being where the next sample should be placed. If our goal is a good reconstruction, the next sample location should be the one that minimizes the expected overall reconstruction error. Let us adopt a common stochastic model [17] and regard the image as a sample function of a continuous 2-D stochastic process, stationary in the wide sense, with correlation that depends exponentially on the distance

$$E[I(x_i,y_i),I(x_j,y_j)] = \sigma^2 e^{-\lambda d_{i,j}} = \sigma^2 e^{-\lambda\sqrt{(x_i-x_j)^2+(y_i-y_j)^2}}. \quad (2.1)$$

Choosing the optimal linear estimator for the image interpolation, it is not difficult to show that the resulting mean square error (MSE) after N samples depends on the sample locations, (x_i,y_i), and is [19]

$$\varepsilon_N^2(x_0\cdots x_{N-1},y_0\cdots y_{N-1}) = \int\int_{\text{Image Area}} (\sigma^2 - \mathbf{V}^T\mathbf{R}^{-1}\mathbf{V})\,dx\,dy \quad (2.2)$$

where

$$R_{i,j} = \sigma^2 e^{-\lambda\sqrt{(x_i-x_j)^2+(y_i-y_j)^2}}$$

and

$$V_i = \sigma^2 e^{-\lambda\sqrt{(x_i-x)^2+(y_i-y)^2}} \quad \text{for all } 0\le i,j\le N.$$

Therefore, the *optimal sampling strategy* after $N-1$ points are sampled would be to choose the Nth sample so that (2.2) is minimized. Note that the expected MSE does not depend on the Nth sample value, but on its location only. This is a direct result of the model's stationarity—the desired sample distribution is uniform, since the statistical properties of the image are spatially constant.

Since minimizing (2.2) is a difficult task, apparently with no analytic solution, let us first consider its one-dimensional (1-D) counterpart. Consider a 1-D stochastic signal $I(x)$ with exponential correlation, defined over the line segment $[a,b]$. Let $S=\{x_i\}_{i=0}^{i=N-1}$ be a set of samples of this signal (for simplicity, we assume that $a,b\in S$). An important property of the exponential correlation model is that the optimal linear estimator $\hat{I}_L(x)$ is invariant to "occluded" sample points (see Fig. 1 for illustration). This property facilitates a closed-form analysis of the 1-D case, since every point $x\in[a,b]$ is occluded from all sample points except two. The expected reconstruction error over the segment between two adjacent sample points x_i, x_j, denoted $\varepsilon^2_{[x_i,x_j]}$, depends therefore only on its length $L=|x_i-x_j|$. Applying (2.2) to this particular case yields

$$\varepsilon^2_{[x_i,x_j]} = \varepsilon_1^2(L) \triangleq \int_{x_i}^{x_j} (\sigma^2 - \mathbf{V}^T\mathbf{R}^{-1}\mathbf{V})\,dx = \sigma^2\left(L\frac{1+e^{-2\lambda L}}{1-e^{-2\lambda L}} - \frac{1}{\lambda}\right). \quad (2.3)$$

It is evident that an additional sample point affects the reconstruction error only in the segment which contains it (see

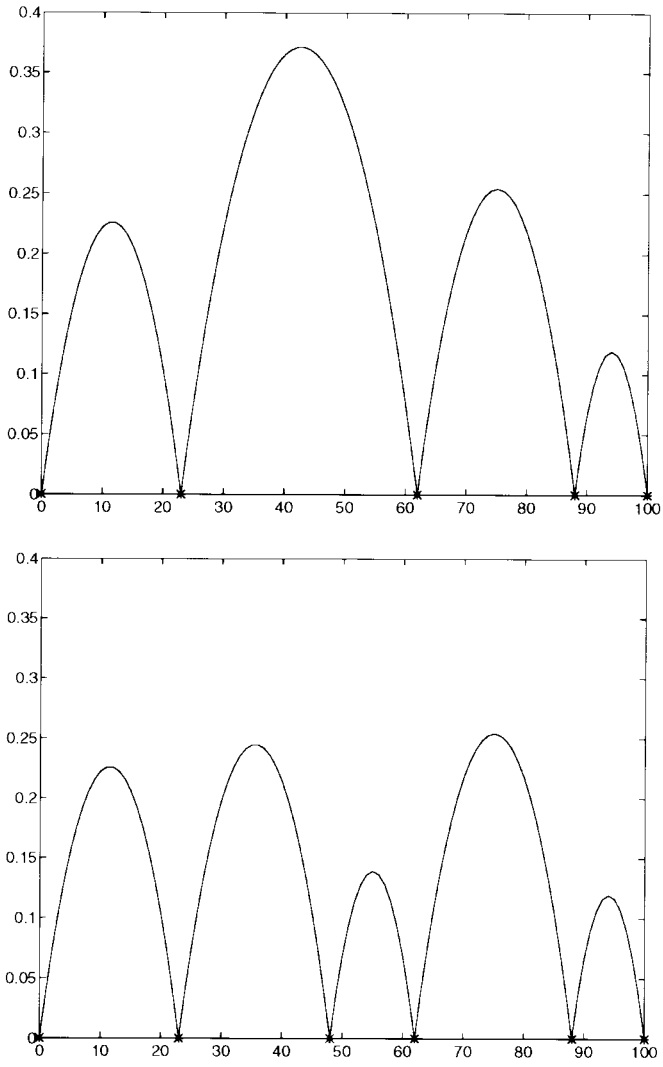

Fig. 2. Illustration of the relatively simple 1-D case: The expected reconstruction error variance at every point before (top) and after (bottom) adding a sample point at $x=48$.

Fig. 2). Adding s_N at distance d from s_i reduces this error by

$$\Delta\varepsilon^2_{[x_i,x_j]}(d) = \varepsilon_1^2(d) + \varepsilon_1^2(L-d) - \varepsilon_1^2(L). \tag{2.4}$$

This function is minimal for $d = \frac{L}{2}$, meaning that s_N should be placed at the middle of an unsampled segment. The decrease of the total reconstruction error is a function of the segment's length L, and is

$$\begin{aligned}\Delta\bar{\varepsilon}^2(L) &= \frac{1}{b-a}\left(2\varepsilon_1^2\left(\frac{L}{2}\right) - \varepsilon_1^2(L)\right) \\ &= \frac{\sigma^2}{b-a}\left(\frac{2L}{e^{\lambda L} - e^{-\lambda L}} - \frac{1}{\lambda}\right).\end{aligned} \tag{2.5}$$

This is a decreasing function of the segment's length L. Hence, the *optimal sampling strategy for the 1-D case* should be as follows: Sample the image at the middle of the longest unsampled line segment, i.e., at the point which is the farthest from the current sample set.

Unfortunately, the 2-D problem cannot be reduced into such a simple form and requires use of numerical minimization techniques. Such an implementation of the optimal strategy is not practical due to its high computational cost. An example of the decrease in the overall reconstruction error, as a function of the location of the next sample point, was calculated using (2.2) and is illustrated in Fig. 3. One may observe the rapid increase of this benefit measure as we move away from the sample points, and that the influence of the distant points seems to be quite small. Inspired by this observation, we approximate the optimal 2-D strategy by augmenting the solution derived for the 1-D case. We suggest the following progressive sampling strategy, FPS.

Definition 2.1—Farthest Point Sampling: Given a sample set $S = \{s_i\}_{i=0}^{i=N-1}$ of an image $I(x,y)$ defined over a region A, the next sample should take place at the point p, which is the farthest from the previous samples, i.e.,

$$\begin{aligned}d(p,S) &= \max_{q\in A}(d(q,S)) \\ &= \max_{q\in A}\left(\min_{0\le i<N}(d(q,s_i))\right).\end{aligned} \tag{2.6}$$

This principle can be interpreted geometrically as follows: The next sample point is the center of the largest empty circle that lies within the image boundaries. It seems that this strategy should be effective for any 2-D data, characterized by a correlation function that decreases with the distance. In this case, the point farthest from the sample set is intuitively the least known one. We have proved it rigorously for a 1-D signal with exponentially decreasing correlation. In the following sections we examine the generated sampling pattern and suggest an efficient algorithm for implementation of the FPS.

III. The Voronoi Diagram

The FPS strategy can be efficiently implemented through incremental construction of a Voronoi diagram (VD). The VD is a well known data structure in computational geometry, widely utilized in the context of proximity problems. In this section we briefly review some of the basic properties of the VD. The discussion is confined to planar points and the Euclidean distance between them, though the VD is well defined for spaces of higher order and with any other metric as well. The Delaunay triangulation (DT) is also reviewed as an introduction to the next section.

Definition 3.2: Let $S = \{s_i\}_{i=0}^{i=N-1}$ be a planar set of points. The *Voronoi cell* of the point $s_i, V(s_i)$, is defined as the set of all planar points that are closer to s_i than to any other point in S. The Voronoi cell is a convex (not necessarily bounded) polygon with no more than $N-1$ sides. The partition of the plane into N Voronoi cells is called the VD of S, $\mathrm{VD}(S)$. The cell's boundaries are defined by the edges of the diagram, and its corners are the diagram's vertices (see Fig. 4).

Definition 3.3: Two points $s_i, s_j \in S$ are *neighboring points* if their Voronoi cells share a common edge.

We shall assume hereinafter that the points s_i are in general position, i.e., no four points lie on the same circle. Under this assumption, the following properties hold.

1) Every Voronoi vertex is the intersection of exactly three edges. This implies that every vertex $v \in \mathrm{VD}(S)$ is the center of a circle $C(v)$ passing through three points of S.
2) For every Voronoi vertex $v \in \mathrm{VD}(S)$ the circle $C(v)$ does not contain any point of S, except the three points it passes through.
3) A Voronoi cell of a point $s \in S$ is not bounded if and only if the point s resides on the boundary of the convex hull of S.

Further information regarding the VD may be found in [2] and [20].

A. The Complexity of VD Construction

Since the problem of vector sorting can be reduced to VD construction for an arbitrary point set, $O(N\log N)$ is a lower bound for the worst case time complexity of the latter task. Shamos [20] suggested a recursive split of S, followed by a merge of the two halves VD's. This algorithm is optimal, but very complex and difficult to implement.

An alternative approach is to build the VD incrementally—starting with the VD of a small subset of S (e.g., three points) and then adding the rest of the points, one at a time, modifying the diagram at each step [5], [13]. The modification stage starts by finding the nearest neighbor to the new point in the current sample set, and then constructing the Voronoi cell of the new point. These algorithms are simple, but offer worst case complexity of $O(N^2)$, meaning that for an arbitrary set of points they are suboptimal. On the other hand, if the points are uniformly distributed (e.g., a sample of a homogeneous Poisson point process), then the expected VD construction time is $O(N\log N)$ [13]. We should point out that the task of finding the nearest neighbor is the one yielding this complexity, while the average time for VD update is constant.

B. The Delaunay Triangulation

A triangulation of a set of planar points S is defined as a set of nonintersecting line segments between the points, dividing the convex hull of S into triangles. A given set of points may have many legal triangulations, but for most applications

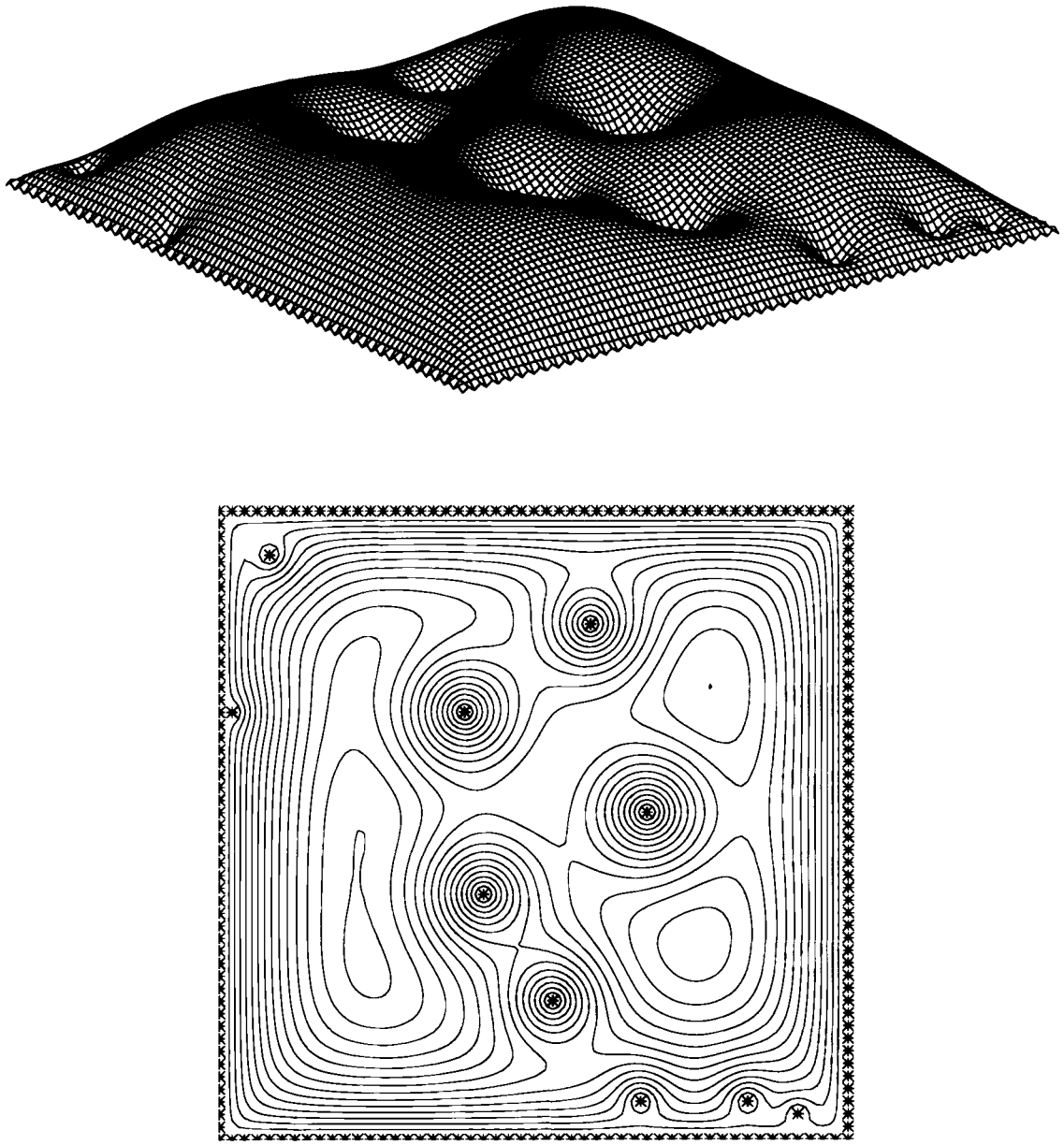

Fig. 3. Decrease in the overall reconstruction error, as a function of the location of the next sample point, computed over a sampled square surface. The surface was sampled densely along its borders and at some other randomly selected points. The same function is described as a three-dimensional (3-D) surface (top) and level-crossing curves (bottom). The dominance of the sampling points (which are indicated by $*$) in its close neighborhood stands out, especially in the second description.

one usually prefers a triangulation which is the closest to an equiangular one. One of the most common criteria is choosing the triangulation in which the smallest angle is maximal (the min-max angle criterion). A good survey of various min-max criteria can be found in [3].

Let T be a triangulation of S. If for each triangle in T the inscribing circle contains no other point of S (except the three points that form the triangle), then T is the Delaunay triangulation, $\mathrm{DT}(S)$. If the above mentioned general position assumption holds, then the DT exists and it is unique. Furthermore, Sibson [24] proved in 1978 that the DT is the optimal triangulation according to the min-max angle criterion. The DT also guarantees the smoothest piecewise linear approximation for a given set of samples [22].

Property 2) of the VD implies a duality between the VD and the DT, i.e. every vertex of the VD corresponds to a triangle in the DT (see Fig. 5). Hence, building $\mathrm{VD}(S)$ provides us with an optimal (equiangular) triangulation of S as well.

IV. The FPS Algorithm and Properties

The FPS, defined in Section II, requires at each stage to find the image point that is the farthest from the current set of sample points S. This task may be executed efficiently using the Voronoi diagram of S, yielding a spatial distribution of the generated sampling pattern, which is uniform in a deterministic sense.

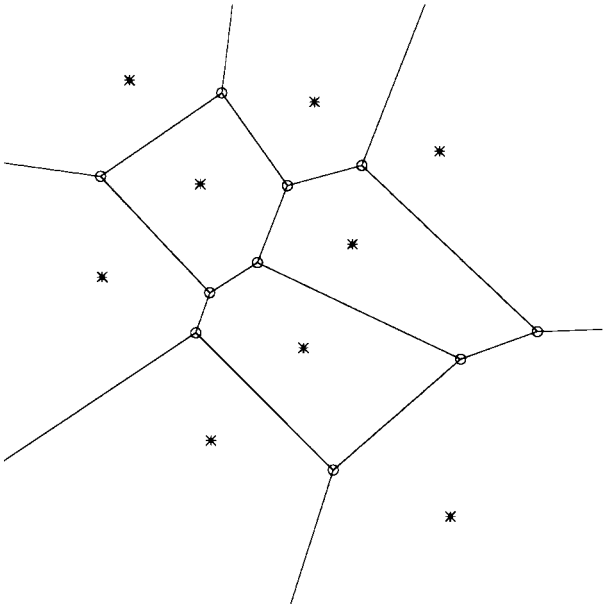

Fig. 4. Voronoi diagram. Sample points are marked with $*$.

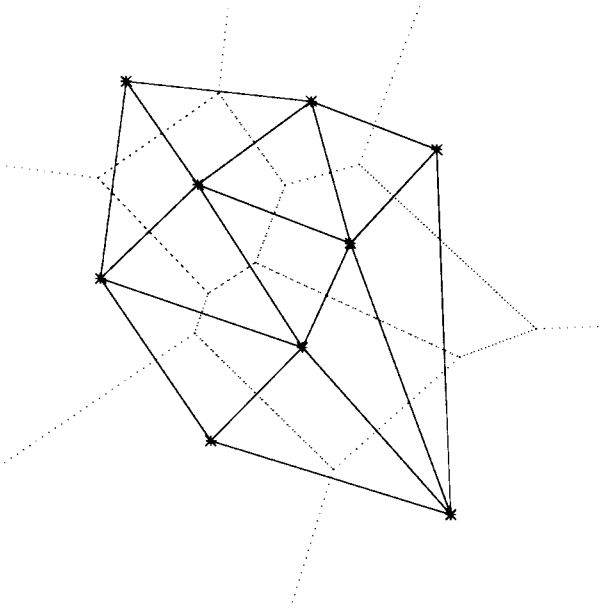

Fig. 5. Delaunay triangulation. Sample points are marked with $*$ and the dotted lines describe the corresponding Voronoi diagram.

Since our domain is finite, we consider a bounded Voronoi cell associated with each sample point, defined as the conjunction of the Voronoi cell with the image definition area. The assembly of all the cells associated with S makes up its bounded Voronoi diagram (BVD) $\mathrm{BVD}(S) = (V, E)$, where E and V are the sets of the diagram's edges and vertices, respectively. For simplicity, let us confine ourselves hereafter to a rectangular image and assume that its corners are sampled.

Consequently, the image is segmented into convex, nonoverlapping, and bounded polygons. Every bounded Voronoi cell contains one sample point and all the image points that are closer to it than to any other sample point, implying the following relation between FPS and the VD.

Theorem 4.1: The point $p \in A$, which is the farthest from the points of the sample set S, lies at a vertex of the BVD of S (for the simple proof, see Appendix B.)

Let us now rephrase the FPS algorithm in terms of the BVD, as follows.

1) Create an initial point set S^5, consisting of the image corners and an additional, randomly chosen point. Calculate $\mathrm{BVD}(S^5) = (V^5, E^5)$. $n = 5$.
2) Find the point $p \in V^n$, which is the farthest from the set of sample points S^n.
3) $S^{n+1} = S^n \cup \{p\}$.
   Calculate $\mathrm{BVD}(S^{n+1})$ [5], [13].
   $n = n + 1$.
4) If more samples are needed, go to 2). The exact stopping rule depends on the application—theoretically, this sampling process could go on indefinitely.

We are now in a position not only to prove that such an implementation is efficient, but also to make some strong claims about the distribution of the sample points. Consider the BVD of the set of sample points S generated by the above described algorithm. Let (V, E) denote the graph associated with $\mathrm{BVD}(S)$. Let $R(v)$ indicate, for every vertex $v \in V$, the distance of the vertex from the nearest sample point, and let v_m, v_M be the closest and farthest vertices to and from S, as follows:

$$R(v) = d(v, S) = \min_{s \in S} d(v, s)$$
$$R_m = R(v_m) = \min_{v \in V - V^5} R(v)$$
$$R_M = R(v_M) = \max_{v \in V - V^5} R(v).$$

Note that distances to V^5 are excluded from the definition of R_M and R_m.

The following theorem introduces deterministic bounds on the distance between sample points and for ratio between the radii of the maximal empty circles associated with the set of sample points. Note that all the theorems in this section were derived for the specific case of a set of points that was generated by the FPS algorithm. They do not hold for the general case of an arbitrary sequence of planar points.

Theorem 4.2:

1) For every set of sample points S which was generated by the algorithm, $R_M \leq 2R_m$.
2) The distance between each pair of sample points $s_i, s_j \in S$ is at least R_M.
3) The distance between neighboring sample points is no more than $2R_M$.

(For proof, see Appendix B.)

Theorem 4.2 expresses the uniformity of the sampling pattern generated by the algorithm. Its first and third parts assure that there will not be any large gaps between the samples, while the second one excludes the possibility of local clustering of sample points. Note that this theorem holds dynamically, i.e., the process may be stopped at any time and will still yield uniformly distributed samples. This deterministic sense of uniformity allows us to make the

following claim, which is crucial for the analysis of the FPS time complexity:

Theorem 4.3: The number of neighboring points (definition 3.3), for every sample point $s \in S$, is bounded (smaller than 24).

(For proof see Appendix B.)

A tighter bound on the number of neighboring points is introduced in Appendix A; But the mere existence of a constant bound (Theorem 4.3), regardless of its value, is sufficient to determine the time complexity of the FPS algorithm.

For this purpose, the above described FPS algorithm may be divided into two tasks—incremental construction of $\mathrm{BVD}(S)$ and finding the farthest Voronoi vertex at every iteration. In the general context of arbitrary point sets,the incremental construction of Voronoi diagram cannot be done at less than $O(N^2)$ time, as claimed by Gowda *et al.* [12] and proved in [10]. The algorithm consists of finding the sample point, which is closest to the new one (for FPS series—one of the corners of the dual Delaunay triangle) and then constructing the bounded Voronoi cell of the new point, edge after edge.

The time complexity of the VD modification, after one point was added, depends on the number of the edges of the Voronoi cell associated with the new point, i.e., the number of its neighboring points. In an arbitrary sequence there may be as many as N neighboring points, yielding $O(N^2)$ complexity for the whole process. On the other hand, the number of neighboring points in an FPS sequence is bounded by a constant value (Theorem A.2), reducing the time complexity of each iteration to $O(1)$.

For efficient implementation of the farthest vertex search we should maintain a balanced binary tree of pointers to the VD vertices, sorted by the vertex distance from the closest sample point. Maintenance of the tree takes $O(N \log N)$ time, yielding $O(N \log N)$ time complexity for the whole FPS algorithm. The existence of such an efficient algorithm should enable integration of the FPS in practical applications.

V. The Anti-aliasing Property of the FPS

The FPS was shown to generate a sequence of uniformly distributed points at every stage, exhibiting high data acquisition rate. In this section we show that the irregularity of this pattern makes it particularly suitable for sampling images designated for visual display.

Regular sampling (i.e., fixed intersample distance) of a spatial signal corresponds to its duplication in the Fourier space. If this signal is not bandlimited, or if it is sampled below its Nyquist rate, the high-frequency components appear at low frequencies and give rise to aliasing. Irregular sampling, on the other hand, corresponds to convolution of the signal with a wideband noise, which has a blurring effect. The coherent duplication of the image in the frequency space yields appearance of semantically significant structures that interfere with its perception much more than noise of the same energy [21].

For example, Fig. 6(a) depicts a densely sampled synthetic image of concentric circles, thinning from the center outwards—i.e. the regions near the image boundary contain higher spatial frequencies. Fig. 6(b) is a zero-order hold reconstruction of this image, obtained from regular sampling on a low-resolution square grid. The aliasing effect stands out, in the form of jagged edges and imaginary circles that may change the semantic interpretation of the image. Fig. 6(c)–(d) depicts reconstructions from the same number of samples placed irregularly. These subsampling methods introduced, instead of false structures, wideband noise—amorphic distortion that fades away the thinner circles but preserves the essential pattern of the image.

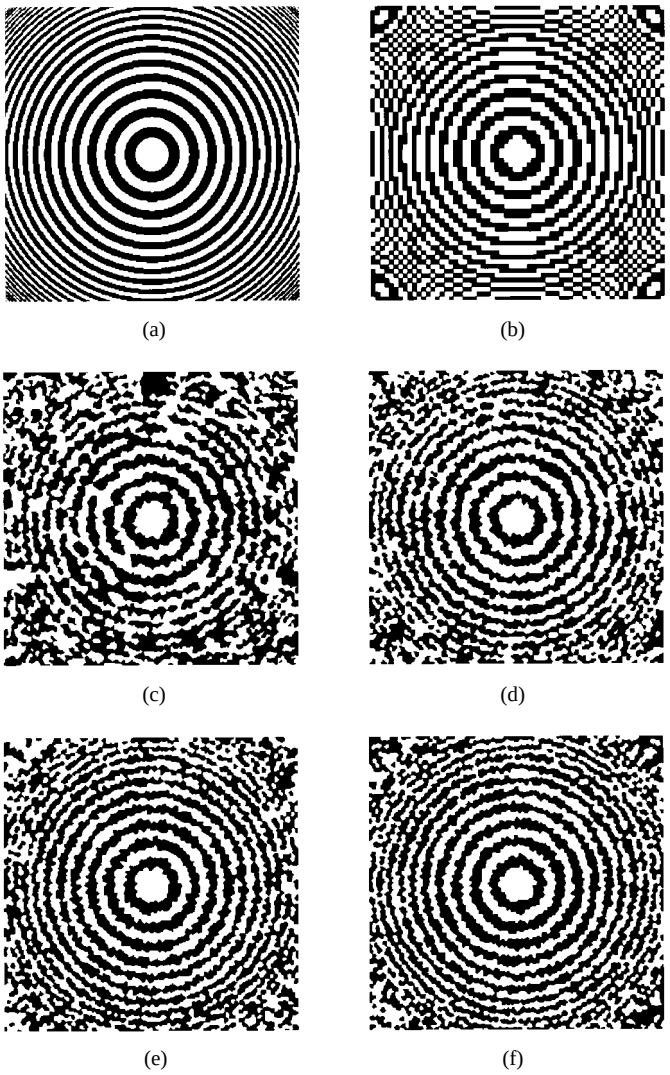

Fig. 6. Reconstructions of an image from various patterns of 4096 sampling point. (a) Original image. (b) Square regular grid ($\mathrm{PSNR} = 6.49$ db). (c) Random (Poisson) distribution ($\mathrm{PSNR} = 4.78$ db). (d) Jittered square grid ($\mathrm{PSNR} = 5.21$ db). (e) Poisson disk distribution ($\mathrm{PSNR} = 5.24$ db). (f) Farthest point sampling ($\mathrm{PSNR} = 5.38$ db). Note that although the signal-to-noise ratio is the highest for the regularly sampled image, its visual appearance is the least faithful to the original (due to aliasing effects).

Anti-aliasing using irregular sampling was mostly investigated in the context of computer graphics. Crow [7] was the first to note that several common defects at computer generated images, such as those shown in the previous example, are caused by the well-known aliasing phenomena. Several studies discussed the prevention of such defects by stochastic

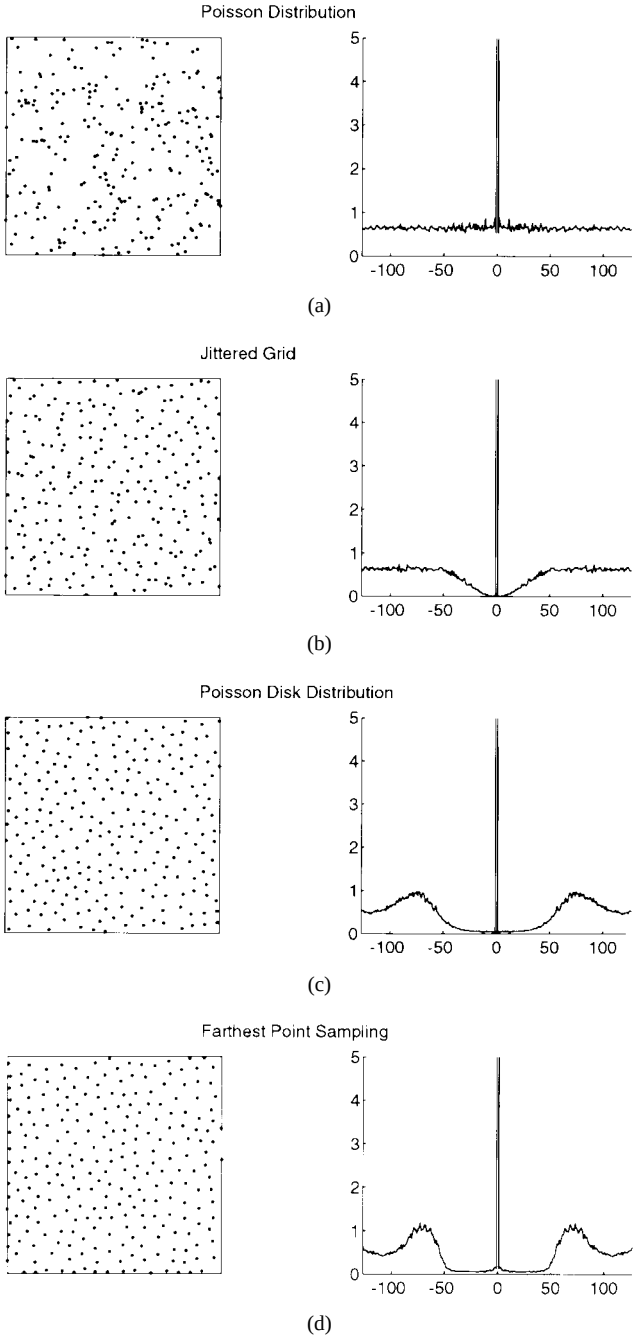

Fig. 7. Stochastic 2-D sampling patterns and their power spectra. (a) Random (Poisson) distribution. (b) Jittered square grid. (c) Poisson disk distribution. (d) Sampling according to farthest point strategy.

distribution of the sample points [6], [8], [15]. The sampling patterns that gave the most visually pleasing results were found to have a "blue" spectrum: There was no power peak at any nonzero frequency (no aliasing), and most of the noise power was concentrated at the high-frequency range, to which the human eye is less sensitive. (This criterion was also introduced at halftoning context [25].) Previous studies focused on three types of stochastic distributions, illustrated at Fig. 7(a)–(c). All those distributions are isotropic, so their energy spectra are radially symmetric and can be displayed as 1-D functions.

The use of Poisson (uniformly) distributed sample points is not common, although it is very simple to generate. Its white spectrum yields prominent, grainy noise, decreasing the visual quality of the reconstructed image. The most popular sampling pattern is generated by jitterring a regular (usually square) grid. The spectral analysis exhibits fairly low power at low frequencies, leading to a much better results than those achieved by Poisson distribution. Nevertheless, the Poisson disk (PD) is undoubtedly the most suitable distribution for image sampling; the points are randomly distributed, provided that the distance between each pair accedes a certain value (the disk diameter). The spectrum of this sampling pattern is characterized by blue noise—almost all of the power is distributed beyond a certain threshold frequency. Generating a Poisson disk distributed set of points is a task of extremely high complexity, which makes it impractical for most applications.

The FPS properties seem to resemble PD constraints in certain respects. The bounded ratio between R_M and R_m guarantees a uniform distribution of the sample points, and the random initialization yields irregularity. Indeed, the power spectrum of the FPS pattern [see Fig. 7(d)] is similar to the one shown at Fig. 7(c). It is radially symmetric (isotropic distribution of the sample points) and most of the power is spread beyond the threshold frequency, as a wideband noise. This spectral character indicates that the pattern is suitable for image sampling, as demonstrated in Fig. 6(f). The reconstructed image matches the one obtained by PD sampling, and outperforms the other methods, while its computational cost is only slightly higher than that of the common Jitter pattern. Another important advantage of the FPS, compared to PD and Jitter, is the possibility to generate additional points progressively, so there is no need to predetermine the required number of samples.

VI. Adaptive FPS

The above described FPS strategy was derived from a stationary image model, leading to the same uniform sampling pattern for every image. For natural images, however, high sample density is needed in areas with finer details while the smoother parts require much lower resolution. More efficient sample distribution can thus be achieved by adopting a nonstationary image model. The next sampling point at each stage should be selected according to the current sample locations and the estimated local bandwidth [16], [26], extracted from the previous sample values.

The most natural augmentation to the FPS would be to define a different metric over the image area, expressing its estimated structure, and to choose the point which is the farthest in this metric. This metric may be derived, for example, from a nonstationary stochastic image model, so that the distance between two points in a high variance region will be greater than the one of an equidistance pair in a smoother region. The main obstacle is that the VD is very difficult to calculate in a non-Euclidean metric—it is well defined, but its edges are not straight lines and finding the farthest point is impractical. We shall therefore restrict ourselves to vertices in the Euclidean VD, choosing at each stage the vertex that maximizes a *weighted distance* function. This new priority function should express both the vertex geometrical distance

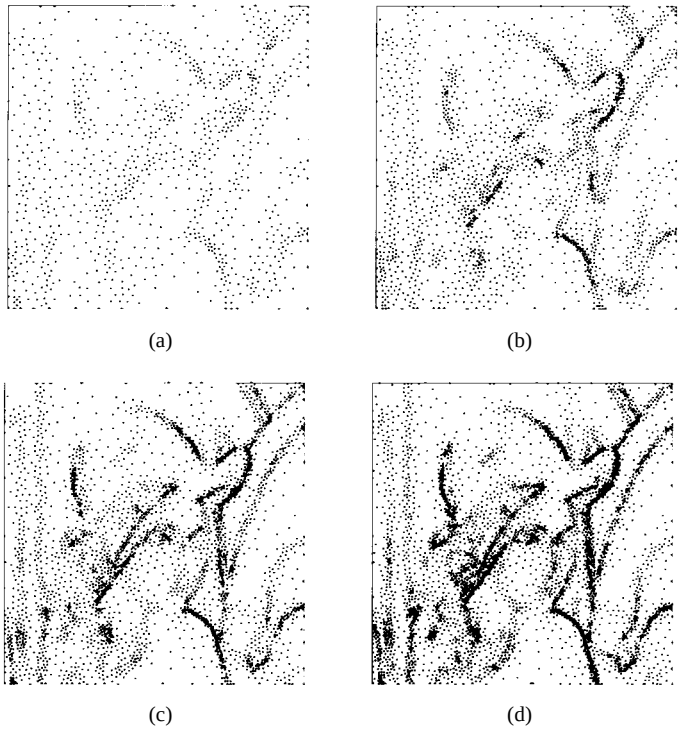

Fig. 8. Progressive construction of the adaptive FPS sampling pattern. (a)–(d) shows the first 1024, 2048, 3072, and 4096 samples, respectively.

from the current sample set and the estimated local bandwidth. We actually approximate the image to be stationary in a the vertex neighborhood—a reasonable assumption for sample sets that are not extremely sparse.

Let us approximate each image region to be a segment of a bounded, bandlimited function. For such function, the Bernstein inequality [1] holds, as follows:

$$|f'(x)| < 2\pi BM \tag{6.1}$$

with B being the function's bandwidth and M—the bound on its amplitude. Calculating the inverse functions to the inequality found in [4], we derive an upper bound for B based on two sample values. Let $I(p), I(q)$ be the image values at points p and q, $I(p) \leq I(q)$, then

$$B \geq B_{\min}(p,q) \tag{6.2}$$

with

$$B_{\min}(p,q) = \frac{\arcsin\left(\frac{2I(q)-M}{M}\right) - \arcsin\left(\frac{2I(p)-M}{M}\right)}{2\pi d(p,q)}.$$

From this bound we derive the suggested weight function

$$W(v) = R^2(v) \max_{s_i,s_j \in N(v)} (B_{\min}(s_i,s_j)) \tag{6.3}$$

Defining the vertex neighborhood $N(v)$ as the closest three sample points, and $R(v)$ being the vertex distance from the current sample set. Note that this is only an example—choosing an appropriate weight function may depend on the specific application, since it reflects some *a priori* knowledge about the image. A more sophisticated approach would have been to construct a time-varying distance function, starting at the Euclidean distance and increasing the adaptivity as the sample density grows.

Experimental results of the adaptive FPS using this function are shown in Figs. 8 and 9. The sample distribution clearly reflects the image structure—samples are denser at regions of high variance (like contours). This weight function, (6.3), gives a good balance between high resolution at areas of interest and reasonable data acquisition over the rest of the image, compared to other weight functions checked [10].

The images in Fig. 9 were all reconstructed from the corresponding sample sets by the same scheme—a weighted average of the four nearest neighbors

$$I(p) = \frac{\sum_{i=1}^{4} \frac{I(s_i)}{d(p,s_i)}}{\sum_{i=1}^{4} \frac{1}{d(p,s_i)}} \tag{6.4}$$

where $\{s_i\}_{i=1}^{i=4}$ are the four sample points which are closest to the center of the pixel p. Since this scheme is not biased toward any of the sampling methods, we believe that the results faithfully reflect their relative differences. Detailed discussion of methods for image reconstruction from irregularly spaced samples is beyond the scope of this paper. Note, however, that K-nearest-neighbors schemes can be implemented very efficiently using the BVD of the sample points. It is evident from Fig. 9 that replacing the Euclidean distance function with the weighted one improves the appearance of the reconstructed image, while preserving the low computational complexity of the algorithm.

VII. Summary and Discussion

According to the farthest point strategy proposed for progressive image sampling, the image should be sampled at each stage at the point which is the farthest from all the previously acquired sample points, i.e., in the center of the largest empty circle.

This sampling strategy has the following attractive properties.

- The generated pattern of sample points is uniform in the sense of having an upper bound on the ratio of distances between the farthest and closest neighboring points. This uniformity criterion is much stronger than the statistical sense of uniformity suggested by previous sampling schemes.
- The number of sample points and the local sampling density change continuously, avoiding the stepwise change characteristic of common pyramidal structures. This implies, among other advantages, that stopping the scan at any arbitrary step always yields the most uniform pattern for the given number of samples. This also stands in contrast to schemes that rely on adaptive subdivision of cells in coarse partitioning, in which the boundary of the large cells are visible.
- The location of sample points is irregular and thus reduces significantly the aliasing effects, implying that the resulting reconstruction from the sampled data is particularly suitable for display. The sampling scheme possesses the

(a) (b)

(c)

Fig. 9. Comparison of reconstructions from sets of 4096 samples with different distributions. (a)–(c): uniform regular sampling on a square grid ($\mathrm{PSNR} = 18.84$ db), uniform FPS ($\mathrm{PSNR} = 18.58$ db) and adaptive FPS ($\mathrm{PSNR} = 18.08$ db). Note again that the PSNR measure fails to reflect the superior visual quality of the FPS-based reconstructions.

"blue noise" characteristic known to be optimal for image display.

- The sampling strategy can be modified to adapt to the content of the sampled image; e.g., more detailed image segments can be sampled more densely. This adaptive version is readily obtained by replacing the distance priority function, which is independent of the image, by some image-dependent or task-dependent priority function.
- An efficient $O(N \log N)$ algorithm, based on the Voronoi diagram corresponding to the sample set, is available for implementing both the uniform and the adaptive scanning processes.
- The pseudorandom sampling pattern is well defined once the locations of the first few sample points are given (also for the adaptive scheme!), allowing for efficient image transmission. This causality feature enables incremental BVD construction at the receiving site too. Transmitting the location of the next sample points is redundant, since their gray values contain this information implicitly.

The sampling scheme presented in this paper is readily available for several applications. A promising direction is its application to ray tracing, where the image of an synthetic world is constructed from a model describing the displayed objects, the light sources, etc. The expected luminance is calculated at a set of sampling points, and the gray level of each pixel is interpolated from the luminance values in its neighborhood. Since evaluating the luminance at each sample points is computationally expensive, the overall rendering time depends heavily on the number of samples taken. Several works suggested stochastic distribution of the sampling points, reducing their number while retaining visual quality of the reconstructed image [6], [8], [15]. The uniformity of the FPS point sequence may allow great reduction of the size of sample set, while the irregularity of the pattern prevents aliasing effects. A parallel ray tracing system using the FPS was already implemented and reported to yield good results, as shown in Fig. 10 [18].

The proposed scheme is in particular attractive for application in progressive transmission of images, which also benefits from both the uniformity and the anti-aliasing properties. Encoding the first few sample point locations, and sending them before transmission of the gray-level information, is a convenient way to encrypt the image (see also [23]). Finally, the farthest point approach may find vast use in the context of

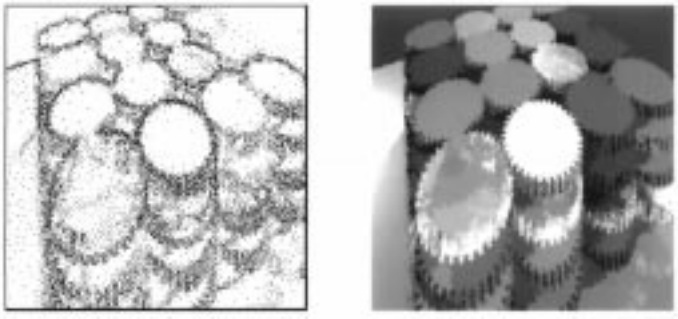

(a) (b)

Fig. 10. Example of the application of the farthest point strategy to image rendering by ray tracing [18]. (a) Locations of the first 10 000 sample points, generated by the adaptive FPS scheme. (b) Reconstructed image.

intelligent vision systems [14]. By using a task-dependent priority function, one can control the scan to enable extraction of specific semantic information, thus implementing a purposive scan.

Appendix A
A Tighter Characterization of the FPS Uniformity

The upper bound on the number of neighboring points, which was introduced in Theorem 4.3, is very loose. In this appendix we introduce a tighter bound on this number and show that the size of the smallest angle in the corresponding DT is also limited. These bounds hold for almost all the points is the FPS sequence, characterizing its uniformity in a deterministic sense.

Recalling the duality between $\mathrm{VD}(S)$ and the Delaunay triangulation $\mathrm{DT}(S)$, we can show that the smallest angle in all $\mathrm{DT}(S)$ triangles is bounded from below.

Theorem A.1: Let S be the set of sample points generated by the FPS algorithm. Let Θ be the set of all the triangles included in $\mathrm{DT}(S)$ and corresponding to Voronoi vertices that lie inside the image boundary. Then

$$\min_{\theta\in\Theta}\theta \geq 25.66^{\circ}.$$

(For proof, see Appendix B.)

The min-max criterion on the angles in a triangulation roughly quantifies the resemblance of the triangles to equiangular ones. Theorem A.1 imposes a lower bound on this measure of equiangularity, and also lets us introduce a tighter bound on the number of neighboring points for samples that are not too close to the image boundary:

Theorem A.2: For every sample point $s \in S$, the distance of which from the image boundary is at least R_M, the number of neighboring points is no more than 14.
(For proof, see Appendix B.)

Note that due to boundary effects, the bounds introduced in Theorems A.1 and A.2 do not apply to all sample points. However, the fraction of samples that do not meet the theorem conditions decreases as the total number of samples is increased.

Appendix B
Theorem Proofs

In this appendix, we prove all the FPS properties claimed above. Note that these claims hold only for point sequences that were generated by the FPS algorithm.

Proof of Theorem 4.1: Let us assume that the farthest point p lies *inside* a BVD cell, corresponding to a sampling point s. The line that starts at s and passes through p intersects the cell boundary at the point q. Since the boundary is a convex and closed polygon, q cannot be between s and p, meaning that $d(q,S) = d(q,s) > d(p,s) = d(p,S)$, which contradicts the fact that p is the farthest point from S. This yields that p must lie on a BVD cell boundary, and for geometrical reasons—at one of its corners, which are BVD vertices. □

Proof of Theorem 4.2:

1) The vertex v_m corresponding to R_m lies at the center of a circle defined by three sample points s_i, s_j, s_k—let us assume without loss of generality that $i < j < k$. Since $v_m \in V - V^5$, then $k > 5$. According to the algorithm, the image is sampled at the point which is the farthest from any existing sample point, hence
$$d(s_k, s_i) \geq \min_{0\leq l<k} d(s_k, s_l) = R_M^k \tag{B.1}$$
where R_M^k, the radius of the largest circle containing no sample point of the k first ones, is a monotonic nondecreasing function, i.e., $R_M^k \geq R_M^n$ for any $n > k$. For $n = N$ we get
$$R_M^k \geq R_M \quad \text{for all } k. \tag{B.2}$$
$$d(s_k, v_m) = d(s_i, v_m) \geq \frac{1}{2} d(s_k, s_i) \tag{B.3}$$
but $d(s_k, v_m) = R_m$, and then, by (B.1, B.2, B.3)
$$R_m \geq \frac{1}{2} d(s_k, s_i) \geq \frac{1}{2} R_M^k \geq \frac{1}{2} R_M. \tag{B.4}$$
2) Let us assume without loss of generality that $j < i$. According to the algorithm s_i lies at v_M^i, i.e., there were no sample points at R_M^i distance from s_i, and in particular $d(s_i, s_j) \geq R_M^i$. In the proof of the previous theorem, we showed that $R_M^i \geq R_M$, hence $d(s_i, s_j) \geq R_M$.
3) Consider two neighboring sample points $s_i, s_j \in S$ that share the two BVD vertices v_k, v_l. Since v_k lies at equal distance from s_i and s_j, a triangular inequality yields $\frac{1}{2} d(s_i, s_j) \leq d(v_k, s_i)$; but by definition $d(v_k, s_i) = R(v_k) \leq R_M$, hence, $d(s_i, s_j) \leq 2R_M$. □

Proof of Theorem 4.3: According to Theorem 4.2, 3), all the neighboring sample points of s lie inside a circle with center at s and $2R_M$ radius. According to Theorem 4.3, the distance between each pair is at least R_M. The maximum number of points that can be placed inside the circle following this constraint is equal to the number of circles with radius $0.5R_M$ that can be placed inside a circle with radius $2.5R_M$. It is easy to introduce a (loose) upper bound to this number by the ratio of circle areas—hence, the number of neighboring points (#NP) is bounded by

$$\#\mathrm{NP} \leq \frac{\pi(2.5R_M)^2}{\pi(0.5R_M)^2} - 1 = 24. \qquad \square$$

Proof of Theorem A.1: Since the full proof of this theorem [10] simple yet quite tedious, we confine ourselves to the guidelines of the proof. Observing the angles between the three sample points s_i, s_j, s_k forming the minimal angle θ and the corresponding VD vertex v, we take advantage of the fact that $d(v, s_i) < d(s_i, s_k)$ [Theorem 4.2, 2)] and, by trigonometric arguments, show that

$$\sin\theta \geq \sin(120^\circ)\frac{R_M}{2R_M} = \frac{\sqrt{3}}{4} \Rightarrow \theta \geq 25.66^\circ. \qquad \square$$

Proof of Theorem A.2: Let s_0 be any sample point and mark its neighboring points $s_1, s_2 \cdots s_k$ so that s_i, s_{i+1} (for any $0 < k < i$) and s_k, s_1 are neighboring points. For any vertex v that belongs to the BVD cell of $s_0, R(v) \leq R_M$ by the definition of R_M, but s_0 is at least R_M away from the image boundary; hence, all these vertices lie within the image boundary and the constraints of Theorem A.1 hold for all the triangles $s_i s_{i+1} v$. Let us denote the angle near s_0 in each of them by θ_i, then $\sum_{i=1}^{k} \theta_i = 360^\circ$. On the other hand, according to Theorem A.1, $\theta_i > 25.66^\circ$ for all i—so the number of neighboring points k is bounded by

$$k \leq \left\lfloor \frac{\sum_{i=1}^{k} \theta_i}{\min_{1 \leq i \leq k} \theta_i} \right\rfloor = \left\lfloor \frac{360}{25.66} \right\rfloor = 14. \qquad \square$$

REFERENCES

[1] N. I. Achieser, *Theory of Approximation*. New York: Frederik Ungar, 1956.

[2] F. Aurenhammer, "Voronoi diagrams—A survey of a fundamental geometric data structure," *ACM Comput. Surveys*, vol. 23, pp. 345–405, 1991.

[3] M. Bern *et al.*, "Edge insertion for optimal triangulations," in *Proc. 1st Latin Amer. Symp. Theoretical Informatics*, Sao Paulo, Brazil, 1992, publ. in *Springer-Verlag Lecture Notes Comput. Sci.*, vol. 583, pp. 46–60.

[4] J. L. de Bougrenet de la Tocnaye and J. F. Cavassilas, "Image coding using an adaptive sampling technique," *Signal Processing: Image Commun.*, vol. 1, pp. 75–80, 1989.

[5] A. Bowyer, "Computing dirichlet tessellations," *Comput. J.*, vol. 24, pp. 162–166, 1981.

[6] R. L. Cook, "Stochastic sampling in computer graphics," *ACM Trans. Graph.*, vol. 5, pp. 137–145, 1986.

[7] F. C. Crow, "The aliasing problem in computer-generated shaded images," *Commun. ACM*, vol. 20, pp. 799–805, 1977.

[8] A. Z. Dippe and E. H. Wold, "anti-aliasing through stochastic sampling," *Comput. Graph.*, vol. 19, pp. 69–78, 1985.

[9] A. Eitan, I. Gertner, and Y. Y. Zeevi, *Image Scanning According to Lines in Finite Fields*. Haifa, Israel: Electr. Eng. Dept., Technion–Isr. Inst. Technol., 1988.

[10] Y. Eldar, "Irregular image sampling using the Voronoi diagram," M.Sc. thesis, Technion–Isr. Inst. Technol., Haifa, Israel, 1992.

[11] I. Gertner, "Image scanning according to lines on finite fields," *SPIE Appl. Digital Image Processing XII*, vol. 1153, pp. 285–293, 1989.

[12] I. G. Gowda, D. G. Kirkpatrick, D. T. Lee, and A. Naaman, "Dynamic Voronoi diagrams," *IEEE Trans. Inform. Theory*, vol. IT-29, no. 5, pp. 724–731, 1983.

[13] P. J. Green and R. Sibson, "Computing dirichlet tessellations in the plane," *Comput. J.*, vol. 21, pp. 168–173, 1978.

[14] O. A. Hilsenrath and Y. Y. Zeevi, "Random access computer vision," *SPIE Vis. Commun. Image Processing II*, vol. 845, pp. 201–206, 1986.

[15] D. P. Mitchell, "Generating antialiased images at low sample densities," *Comput. Graph.*, vol. 21, pp. 65–72, 1987.

[16] M. Porat and Y. Y. Zeevi, "The generalized Gabor scheme in biological and machine vision," *IEEE Trans. Pattern Anal. Machine Intell.*, vol. 10, pp. 452–468, 1988.

[17] A. N. Netravali and B. G. Haskell, *Digital Pictures*. New York: Plenum, 1988.

[18] I. Notkin and C. Gotsman, "Parallel progressive ray-tracing," *Comput. Graph. Forum*, vol. 16, no. 1, 1997; also *CIS Rep. 9416*, Technion–Isr. Inst. Technol., Haifa, Israel, 1994.

[19] A. Papoulis, *Probability, Random Variables, and Stochastic Processes*. New York: McGraw-Hill, 1984.

[20] F. P. Preparata and M. I. Shamos, *Computational Geometry*. New York: Springer-Verlag, 1985.

[21] H. L. Resnikoff, "The duality between noise and aliasing and human image understanding," *SPIE Image Understanding Man–Machine Interface*, vol. 758, pp. 31–38, 1987.

[22] S. Rippa, "Minimal roughness property of the delaunay triangulation," *Comput. Aided Geometr. Des.*, vol. 7, pp. 489–497, 1990.

[23] H. Rom and S. Peleg, "Image representation using Voronoi tessellation: Adaptive and secure," *CVPR*, pp. 282–285, 1988.

[24] R. Sibson, "Locally equiangular triangulations," *Comput. J.*, vol. 21, pp. 243–245, 1978.

[25] R. Ulichney, *Digital Halftoning*. Cambridge, MA: MIT Press, 1987.

[26] Y. Y. Zeevi and E. Shlomot, "Non-uniform sampling and anti-aliasing in image representation," *IEEE Trans. Signal Processing*, vol. 41, pp. 1223–1236, 1993.

Yuval Eldar received both the B.Sc. degree in computer engineering and M.Sc. degree in electrical engineering from the Technion–Israel Institute of Technology, Haifa, Israel, in 1989 and 1992, respectively.

Since 1994, he has been with IBM Israel Science and Technology Center, Haifa. His research interests are in the area of computer vision, especially data acquisition processes.

Michael Lindenbaum (M'97) was born in Israel in 1956. He received the B.Sc., M.Sc., and D.Sc. degrees in the Department of Electrical Engineering at the Technion–Israel Institute of Technology (IIT), Haifa, in 1978, 1987, and 1990, respectively. He performed post-doctoral work at the NTT Basic Research Laboratories, Tokyo, Japan

From 1978 to 1985, he served in the IDF. Since October 1991, he has been with the Department of Computer Science, IIT. His main research interest is computer vision, and especially statistical analysis of object recognition and grouping processes.

Moshe Porat (S'86–M'87–SM'97) received the B.Sc. (summa cum laude) and D.Sc. degrees, both in electrical engineering, from the Technion–Israel Institute of Technology (IIT), Haifa, in 1982 and 1987, respectively.

Since 1988, he has been with the Faculty of Electrical Engineering, IIT. During 1991–1992, he was with the Signal Processing Department at AT&T Bell Laboratories, Murray Hill, NJ, on leave from IIT. His professional interests are in the area of human and machine vision, specializing in localized representations of signals for image processing and computer vision.

Yehoshua Y. Zeevi received the undergraduate degree from the Technion–Israel Institute of Technology (IIT), Haifa, the M.Sc. from the University of Rochester, Rochester, N.Y., and the Ph.D. from the University of California, Berkeley.

He is the Barbara and Norman Seiden Professor of Computer Sciences and the Dean of the Faculty of Electrical Engineering, IIT. He was a Vinton Hayes Fellow at Harvard University, Cambridge, MA, and has been a regular visitor there. He was also a Visiting Professor at the Massachusetts Institute of Technology, Cambridge, and at the Computer Aids for Industrial Productivity Center, Rutgers University, New Brunswick, NJ. His major research is devoted to image representation, visual communication, and biological and computer vision. He is one of the founders of i Sight, Inc., a company devoted to digital video cameras that mimic visual systems and real-time image processing.

Dr. Zeevi is the Editor-in-Chief of the *Journal of Visual Communication and Image Representation* and a member of editorial boards of several other journals.